Article

Highly Sensitive, Selective, Flexible and Scalable Room-Temperature NO$_2$ Gas Sensor Based on Hollow SnO$_2$/ZnO Nanofibers

Jiahui Guo [1,2] , **Weiwei Li** [3,4], **Xuanliang Zhao** [2], **Haowen Hu** [2], **Min Wang** [2], **Yi Luo** [1], **Dan Xie** [4,*], **Yingjiu Zhang** [1,*] and **Hongwei Zhu** [2,*]

1   Key Laboratory of Material Physics, Ministry of Education, School of Physics and Microelectronics, Zhengzhou University, Zhengzhou 450052, China; guojiahuizzu@163.com (J.G.); luoyilogic@163.com (Y.L.)
2   State Key Laboratory of New Ceramics and Fine Processing, School of Materials Science and Engineering, Tsinghua University, Beijing 100084, China; zhao-xl15@mails.tsinghua.edu.cn (X.Z.); haowenh6677@126.com (H.H.); wangmin199303@163.com (M.W.)
3   Department of Basic Sciences, Air Force Engineering University, Xi'an 710051, China; kgdliweiwei@163.com
4   Beijing National Research Center for Information Science and Technology (BNRist), Institute of Microelectronics, Tsinghua University, Beijing 100084, China
*   Correspondence: xiedan@tsinghua.edu.cn (D.X.); zhangyj2006@zzu.edu.cn (Y.Z.); hongweizhu@tsinghua.edu.cn (H.Z.)

Abstract: Semiconducting metal oxides can detect low concentrations of NO$_2$ and other toxic gases, which have been widely investigated in the field of gas sensors. However, most studies on the gas sensing properties of these materials are carried out at high temperatures. In this work, Hollow SnO$_2$ nanofibers were successfully synthesized by electrospinning and calcination, followed by surface modification using ZnO to improve the sensitivity of the SnO$_2$ nanofibers sensor to NO$_2$ gas. The gas sensing behavior of SnO$_2$/ZnO sensors was then investigated at room temperature (~20 °C). The results showed that SnO$_2$/ZnO nanocomposites exhibited high sensitivity and selectivity to 0.5 ppm of NO$_2$ gas with a response value of 336%, which was much higher than that of pure SnO$_2$ (13%). In addition to the increase in the specific surface area of SnO$_2$/ZnO-3 compared with pure SnO$_2$, it also had a positive impact on the detection sensitivity. This increase was attributed to the heterojunction effect and the selective NO$_2$ physisorption sensing mechanism of SnO$_2$/ZnO nanocomposites. In addition, patterned electrodes of silver paste were printed on different flexible substrates, such as paper, polyethylene terephthalate and polydimethylsiloxane using a facile screen-printing process. Silver electrodes were integrated with SnO$_2$/ZnO into a flexible wearable sensor array, which could detect 0.1 ppm NO$_2$ gas after 10,000 bending cycles. The findings of this study therefore open a general approach for the fabrication of flexible devices for gas detection applications.

Keywords: electrospinning; tin oxide nanofibers; zinc oxide; gas sensor; flexible devices

1. Introduction

Nitrogen dioxide (NO$_2$), one of the most hazardous gases, poses a great threat to humans, animals, and plants [1–3]. It may induce various illnesses in humans even at very low concentrations. In addition, the excessive emission of NO$_2$ gas causes numerous environmental problems, such as surface water acidification and photochemical smog [4,5]. Therefore, the detection of NO$_2$ gas is critical for human health and environmental conservation. The interest in semiconducting metal oxides has grown in recent years owing to their good performance in the optical, electronic and gas sensor fields. Semiconducting metal oxides such as SnO$_2$, ZnO, In$_2$O$_3$, TiO$_2$, and NiO have the advantages of good chemical stability, excellent sensitivity, low cost, and easy fabrication. Therefore, these semiconductors have been widely investigated and applied in NO$_2$ gas detection [6–11]. There are various ways of improving the detection efficiency of these materials, such as the

application of an electrostatic field [12], doping with other nanomaterials [13], and ultra-violet (UV) illumination [14,15]. Of these techniques, nanomaterials doping is attracting increasing attention as an effective strategy.

SnO_2 and ZnO, as typical n-type semiconductors, have been widely regarded as effective and practical gas sensing materials over the past decade [16]. However, most studies on the gas sensing properties of SnO_2 and ZnO have been carried out at high temperature. Accordingly, it is still challenging to fabricate SnO_2- and ZnO-based NO_2 gas sensors with excellent sensing performances at room temperature. Therefore, several reasonable approaches have been used with the aim of improving their sensing properties, including doping with metals [17] and carbon materials [18], and surface modification using Pt, Ag particles [19,20]. SnO_2 and ZnO nanocomposites are deemed to be effective materials for improving gas sensing properties [16,21,22]. Sunghoon et al. fabricated SnO_2-Core/ZnO-shell nanowires and found a response of about 239% towards 1 ppm of NO_2 gas [20]. Yang et al. also fabricated ZnO-SnO_2 heterojunction nanobelts that showed a faster response (1.8 s)/recovery (18 s) speed to triethylamine [22]. Although ZnO-SnO_2 nanocomposites have been prepared and modified to improve sensing performance, room temperature chemical sensors still face great challenges during application. In this study, a novel SnO_2/ZnO nanocomposite with excellent sensing performance at room temperature was prepared. Its sensing properties and mechanism at room temperature were then investigated. Moreover, due to the increased development of wearable electronic devices, it is logical to study flexible wearable gas sensors [23,24]. However, flexible gas sensors usually involve transfer of the prepared substrate layers or even the whole device onto special flexible substrates, as well as the attachment of target gases, limiting their practical applications. Therefore, it would be necessary to develop a facile, flexible, and scalable gas sensor preparation method.

Herein, hollow SnO_2/ZnO nanofibers were synthesized by a facile electrospinning and calcination method. The gas sensing performance and mechanism of gas sensors based on pristine SnO_2 and SnO_2/ZnO nanocomposite were also investigated at room temperature. The results revealed that the SnO_2/ZnO nanofibers coated on titanium/gold interdigital electrodes exhibited high sensitivity and selectivity to NO_2 gas sensing at ppb level, and at a minimum detection limit of 0.1 ppm during testing. SnO_2/ZnO sensors exhibited high sensitivity to 0.5 ppm NO_2, with a response value of 336% and a fast response time of <2 min, all of which relied on both physisorption and chemisorption-based charge transfer. Furthermore, patterned silver paste electrodes were printed on different flexible substrates including paper, polyethylene terephthalate (PET) and polydimethylsiloxane (PDMS) by using screen printing. These were then integrated with SnO_2/ZnO nanofibers as sensing layers into a novel flexible and wearable gas sensor. After 10,000 bending cycles, the SnO_2/ZnO flexible gas sensor did not lose its high sensitivity properties for the detection of NO_2 gas.

2. Experimental Section

2.1. Materials

N-dimethylformamide (DMF), stannous chloride ($SnCl_4 \cdot 2H_2O$), and zinc nitrate hexahydrate ($Zn(NO_3)_2 \cdot 6H_2O$) were purchased from Alfa Aesar. Poly (vinylpyrrolidone) (PVP, M_w = 1,300,000) was obtained from Sigma-Aldrich. Ethanol and silver paste were supplied by Sinopharm Chemical Reagents (Shanghai, China), and Beijing NANOTOP Co. Ltd. (Beijing, China), respectively.

2.2. Synthesis of Hollow SnO₂ and SnO₂/ZnO Nanofibers

The transparent precursor solution for the synthesis of SnO_2 nanofibers was prepared by addition of 0.6 g $SnCl_4 \cdot 2H_2O$ into 10 mL ethanol/DMF (volume ratio 1:1) solvent mixture, in which 0.8 g PVP had already been dissolved. In the preparation of SnO_2/ZnO nanofibers, 0.005 g, 0.01g and 0.03 g $Zn(NO_3)_2 \cdot 6H_2O$ were respectively added into two bottles of the precursor solution mentioned above, and the corresponding prepared samples

labeled SnO$_2$/ZnO-1, SnO$_2$/ZnO-2, and SnO$_2$/ZnO-3, respectively. The precursor solution was magnetically stirred at room temperature for 3 h until a clear and transparent solution was formed. A 2 mL volume of precursor solution was then drawn using a 5 mL syringe with a stainless steel needle for electrospinning. The needle was connected to the positive pole, and the negative pole was connected to an aluminum foil, which was placed 20 cm away from the collector, as shown in Figure 1a. The electrospinning parameters used were as described below: the voltage was 20 kV, the humidity range was 40–50% relative humidity (RH), and the collection time was 2 h. The electrospun fibers were then calcinated at 600 °C for 3 h at a heating rate of 10 °C/min.
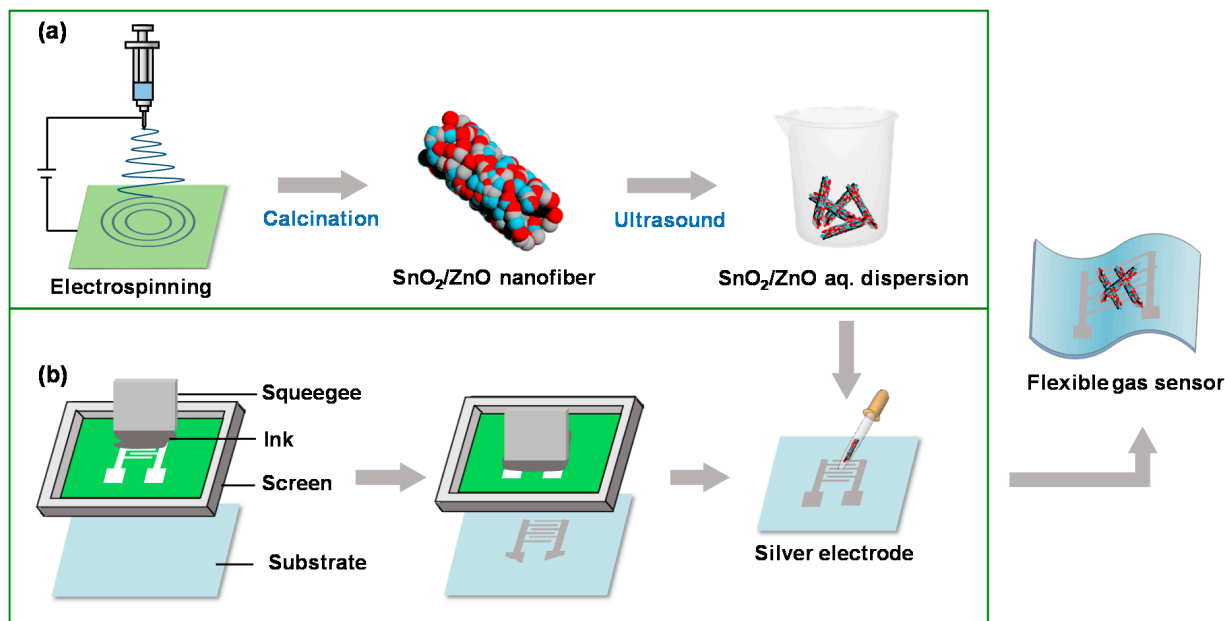

Figure 1. (**a**) Schematic diagrams of the preparation process of SnO$_2$/ZnO composite nanofibers by electrospinning. (**b**) Fabrication process of flexible electrodes by screen printing with silver paste on substrates.

2.3. Fabrication of Flexible Patterned Electrodes

A screen plate with patterned electrodes was fixed on a commercial screen-printing press. The different substrates (paper, PET, PDMS) were placed about 5 cm below the screen plate. Silver paste was then pressed along the patterns using a squeegee at a constant speed to form a clear and flat flexible electrode traces on the substrate, as shown in Figure 1b. The flexible substrates with silver electrodes were dried in the oven at 120 °C for 0.5 h after fabrication.

2.4. Preparation and Test of Gas Sensors

Titanium/gold (Ti/Au) interdigital electrodes, with gaps and finger widths of both 10μm, were fabricated on silicon/silicon dioxide (Si/SiO$_2$) substrates by lithography. The flexible electrodes deposited on paper, PET and PDMS by screen printing had a gap and finger widths of 0.1 mm. Sensing nanofibers were then dispersed in deionized (DI) water, followed by drop-coating onto the electrodes (Figure 1b). The gas sensing properties were evaluated using a homemade system at room temperature (~20 °C). This system could monitor the changes in resistance in dynamic variation process of gas concentration controlled by mass flow controller. The resistance values were recorded using Keithley 2700, China. The response values were then calculated using Equation (1):

$$S\,(\%) = (R_a - R_g)/R_a \times 100\% \tag{1}$$

where R_a is the initial resistance of air and R_g is the resistance of the target gas. The response and recovery time were 90% of the time when the resistance reached its maximum in the target gas and the minimum in the air, respectively.

2.5. Characterizations

The hollow SnO_2 nanofibers, SnO_2/ZnO composite nanofibers were characterized by scanning electron microscopy (SEM, JSM-7401F, JEOL, Akishima, Japan), transmission electron microscopy (TEM, JEM-2010, JEOL, Tokyo, Japan), electron dispersive spectroscopy (EDS) installed in TEM, X-ray photoelectron spectroscopy (XPS, PHI-5300, Perkin-Elmer, Waltham, MA, USA) using AlKα radiation (hν = 1486.6 eV), and specific surface area analyzer (Autosorb-iQ2-MP, Quantachrome, Shanghai, China). The change in resistance of the silver electrodes during bending cycles was recorded using a stretcher (INSTRON 5943, Instron, Shanghai, China).

3. Results and Discussion

3.1. Characterizations of SnO_2, SnO_2/ZnO Nanofibers

The process of SnO_2/ZnO composite nanofiber preparation is illustrated in Figure 1a. Humidity is a very important factor in the electrospinning process. Low humidity causes the blockage of electrospinning needle, whereas high humidity makes it difficult to collect samples at the collector. Figure 1b displays the fabrication process of flexible electrodes through screen printing using silver paste on different substrates. The fabrication process was strongly influenced by the physical properties of silver paste, especially the viscosity and the organic solvents used. The appropriate organic solvent enabled silver paste to be cured at room temperature. High viscosity was essential in preventing excessive spreading on the substrate, whereas high-viscosity silver paste was not compatible with other printing techniques, such as gravure [25] and inkjet [26].

SEM images of the electrospun SnO_2/PVP, $SnO_2/ZnO/PVP-1$, $SnO_2/ZnO/PVP-2$, and $SnO_2/ZnO/PVP-3$ nanofibers are shown in Figure 2a–d. The diameters of these fibers were found to be similar to each other, and their surface morphology appeared to be smooth because of the features of the polymer used. SEM images of hollow SnO_2, $SnO_2/ZnO-1$, $SnO_2/ZnO-2$, and $SnO_2/ZnO-3$ nanofibers after calcination were as shown in Figure 2e–h. The surface of the nanofibers was clearly concave–convex and porous after calcination treatment, and the nanofibers consisted of nanoparticles. By comparing these images, it was revealed that the morphologies of all the hollow nanofibers were porous, and their diameters exhibited almost no significant difference ($d = 180 \pm 20$ nm). Therefore, it can be inferred that the slight difference in diameters between SnO_2, SnO_2/ZnO nanofibers may not have an appreciable effect on their sensing performance.
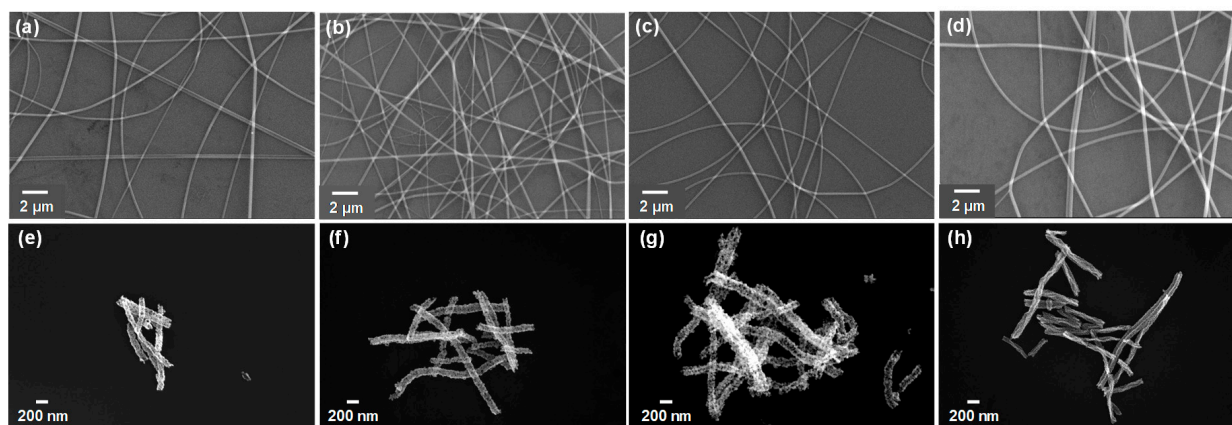

Figure 2. SEM images of (**a**) pristine SnO_2/PVP, (**b**) $SnO_2/ZnO/PVP-1$, (**c**) $SnO_2/ZnO/PVP-2$, (**d**) $SnO_2/ZnO/PVP-3$ before calcination. (**e–h**) Corresponding SEM images of porous hollow SnO_2, $SnO_2/ZnO-1$, $SnO_2/ZnO-2$, $SnO_2/ZnO-3$ nanofibers after calcination, respectively.

To further verify the structure of SnO_2/ZnO composite nanofibers, TEM images were taken from the as-prepared SnO_2/ZnO-3 sample. The TEM images in Figure 3a and its inset show porous structures with a mean diameter of 112.8 nm. As shown in Figure 3b, the interplanar spacing was 0.34 nm for the SnO_2 (110) plane and 0.27 nm for the ZnO (100) plane, which were in accordance to a previous study [26]. This result illustrated that SnO_2/ZnO composite nanofibers fabricated consisted of SnO_2 and ZnO nanoparticles of different sizes ($d = 10 \pm 5$ nm), which had a significant effect on the gas sensing properties of the nanofibers. The response performance decreased with the increase of grain size and exited from the optimal grain size range [27]. The grain size of SnO_2 and ZnO nanoparticles prepared in this study was just in the optimal range. To investigate the chemical composition of SnO_2/ZnO composite nanofibers, element mapping images were also measured. As shown in Figure 3c, the O (white), Sn (green) and Zn (red) atoms were uniformly distributed throughout the SnO_2/ZnO nanofibers. Moreover, the percentage of Sn atoms was found to be more than that of O and Zn, with Zn being the least.
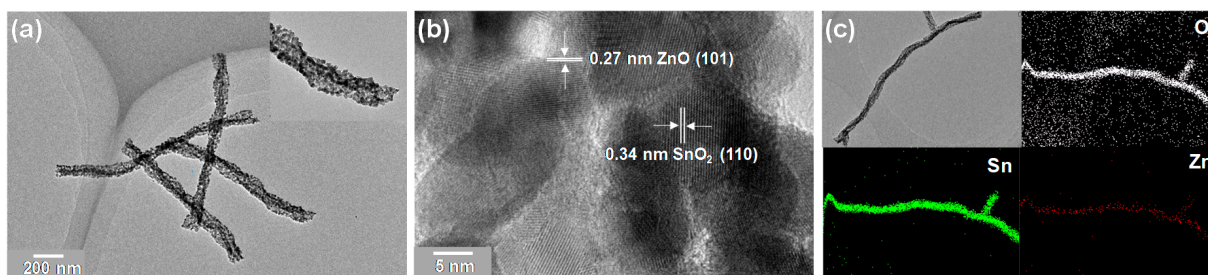

Figure 3. (**a**,**b**) TEM images of SnO_2/ZnO-3 composite nanofibers. The inset of (**a**) is the enlargement. (**c**) Elemental mappings of SnO_2/ZnO-3 composite nanofibers.

The surface chemical composition of SnO_2/ZnO-2 composite nanofibers was further characterized using XPS. As shown in Figure 4a, the peaks of Sn, Zn, O, and C were all observed, and no other impurities were detected. The two peaks that emerged in Figure 4b, located at 486.4 and 494.8 eV with a separation of 8.4 eV, corresponded to Sn $3d_{5/2}$ and Sn $3d_{3/2}$ of Sn^{4+} ions, respectively. The two peaks that appeared at a binding energy of 1044.9 and 1021.9 eV in Figure 4c corresponded to Zn $2p_{1/2}$ and Zn $2p_{3/2}$ of Zn^{2+} ions, respectively [28,29]. From Figure 4d, it can be seen that the O 1s spectrum consisted of two different components at 530.27 eV and 531.60 eV, corresponding to the lattice oxygen in ZnO and the lattice oxygen in SnO_2, respectively. These results further demonstrate that SnO_2/ZnO composite nanofibers were formed from SnO_2 and ZnO nanoparticles [30].

The fabrication process of hollow SnO_2 nanofibers has been previously outlined [31]. During the annealing process, due to the decomposition of PVP template, Sn precursors are rapidly oxidized and redistributed through surface diffusion to form SnO_2 nanoparticles, which is a component of the hollow nanofibers. Similarly, Sn and Zn precursors will be oxidized to form SnO_2 and ZnO nanoparticles during the calcination process. The data shown in Table 1 point to the conclusion that moderate doping of ZnO remarkably promotes the Sn precursors oxidation, leading to the formation of more SnO_2 nanoparticles. Moreover, the surface area of SnO_2/ZnO composite nanofibers is larger than that of pure SnO_2 nanofibers, and thus it is prone to providing more active sites for the adsorption and desorption of gas molecules [28]. Additionally, the surface area of SnO_2/ZnO increases with the concentration of ZnO. Therefore, the SnO_2/ZnO composite nanofibers were expected to have enhanced gas sensing properties.
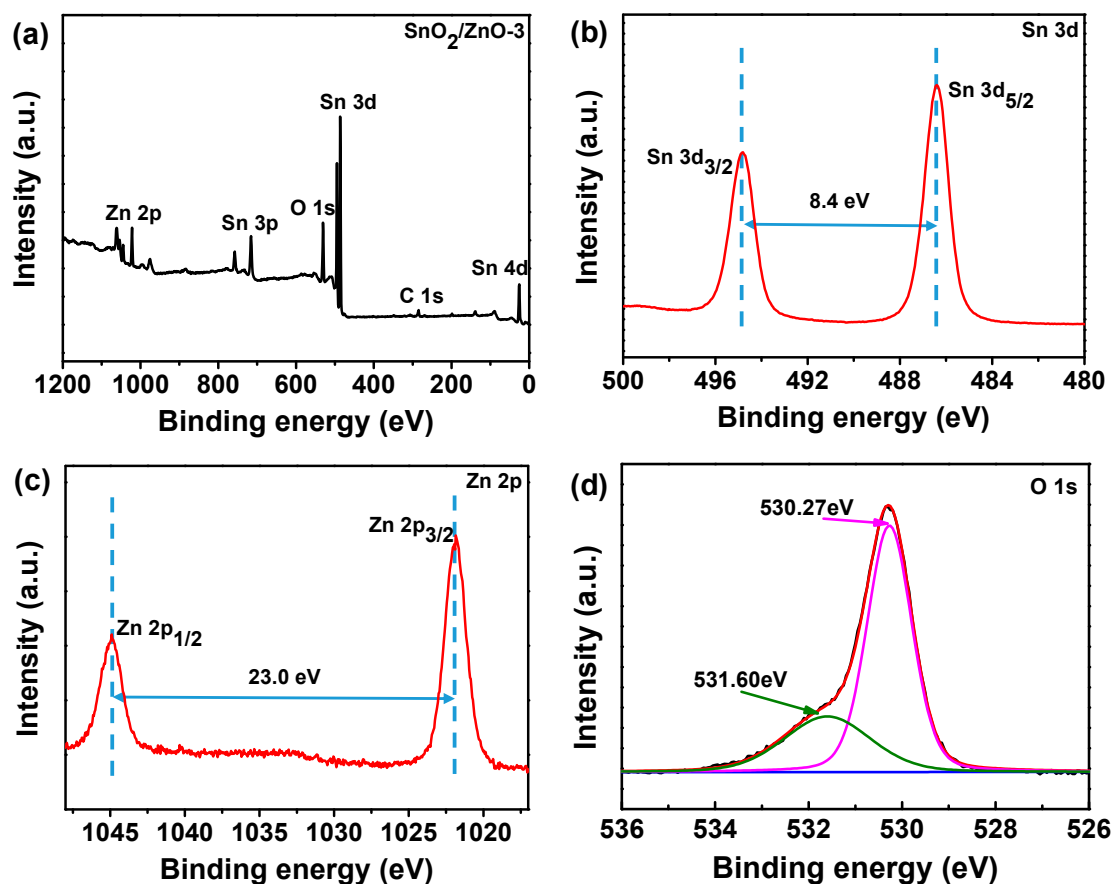
Figure 4. (**a**) Survey, (**b**) Sn 3d, (**c**) Zn 2p, (**d**) O 1s XPS spectra of SnO_2/ZnO-3 composite nanofibers.

Table 1. The content of Sn, Zn, O, and C elements, and the specific surface area of SnO_2, SnO_2/ZnO-1, SnO_2/ZnO-2, and SnO_2/ZnO-3.

Samples	Sn (at.%)	Zn (at.%)	O (at.%)	C (at.%)	Specific Surface Area (m^2/g)
SnO_2	18.6	-	51.8	29.6	28.3
SnO_2/ZnO-1	23.9	1.3	58.4	16.4	31.2
SnO_2/ZnO-2	23.9	3.5	59.1	13.5	35.8
SnO_2/ZnO-3	22.9	8.2	55.6	13.3	38.7

3.2. Gas Sensing Properties of SnO₂, SnO₂/ZnO Composite Nanofibers

The gas sensing properties of SnO_2, SnO_2/ZnO-1, SnO_2/ZnO-2 and SnO_2/ZnO-3 at different concentrations of NO_2 gas at room temperature were studied. Figure 5 shows that the resistance increased upon exposure to NO_2 gas and recovered completely to the initial resistance value upon the removal of NO_2. This indicates that the SnO_2 and SnO_2/ZnO gas sensors had good and stable reversibility. The response values of pure SnO_2 gas sensor exposed to 0.1, 0.5, 5, 10 and 20 ppm of NO_2 gas were 8%, 13%, 24%, 34% and 45%, respectively. Meanwhile, the response values of the SnO_2/ZnO-1 sensor, successively, were 13.2%, 22.9%, 49.0%, 61.1%, 95.5%. For the SnO_2/ZnO-2 sensor, the response values obtained were 21%, 28%, 68%, 116% and 173%, respectively, which is almost three times higher than the values obtained for the pure SnO_2 gas sensor. In comparison to SnO_2/ZnO-1 and SnO_2/ZnO-2, the SnO_2/ZnO-3 sensor possessed the best sensing performance, with a response value of 1945% to 20 ppm of NO_2 at room temperature. Figure 5d shows the response values of the SnO_2/ZnO-3 gas sensor to 0.1, 0.5, 5 and 10 ppm of NO_2, which were 122%, 336%, 895% and 1384%, respectively.
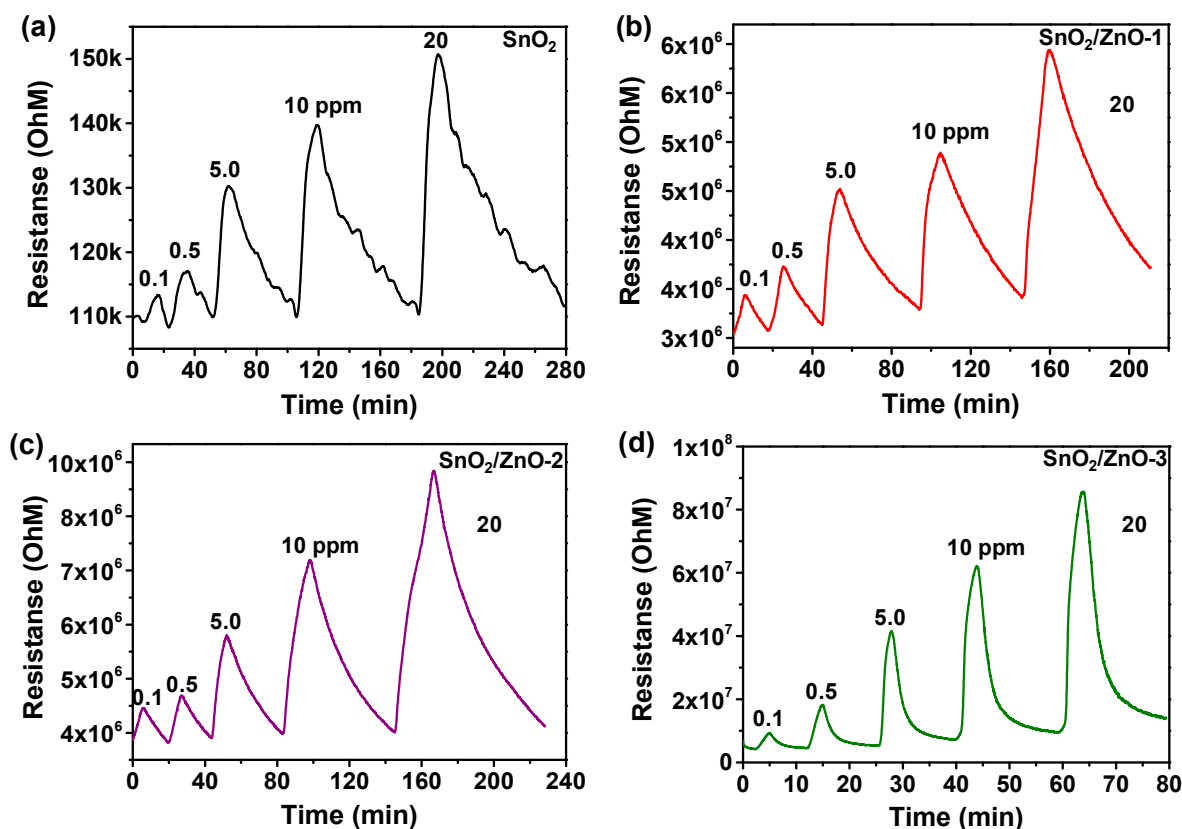
Figure 5. Dynamic responses of (**a**) pristine SnO_2, (**b**) SnO_2/ZnO-1, (**c**) SnO_2/ZnO-2, (**d**) SnO_2/ZnO-3 nanofibers to different concentrations of NO_2 gas (0.1, 0.5, 5, 10, 20 ppm) at room temperature.

The responses of SnO_2, SnO_2/ZnO-1, SnO_2/ZnO-2 and SnO_2/ZnO-3 gas sensors are shown in Figure 6a. The response of SnO_2/ZnO was found to be better than that of pure SnO_2 nanofibers, and it had the tendency of rising more rapidly when NO_2 gas concentration increased. A comparison of NO_2 gas sensing properties of different materials is shown in Table 2. From the table, it can be seen that SnO_2/ZnO sensors exhibited high sensitivity to 0.5 ppm of NO_2 with a response value of 336% and a faster response time of <2 min. Therefore, the response performance of SnO_2/ZnO gas sensor was found to be remarkably higher than those of reported NO_2 gas sensors. To further visually observe the NO_2 sensing properties of the SnO_2/ZnO-3 gas sensors at room temperature, the linear range for NO_2 detection is as displayed in Figure 6b. From this figure, it can be seen that with a rise in gas concentration, there was a gradual increase in response. From Figure 6c, the response and recovery times of SnO_2/ZnO-3 gas sensors to 0.5 ppm of NO_2 at room temperature were 2.1 and 4.0 min, respectively. The response and recovery time of gas sensors based on as-prepared samples to 0.5 ppm of NO_2 was as presented in Figure 6d. From this figure, it can be seen that the response/recovery time gradually decreased with the increase in the amount of ZnO doped. When compared with existing gas sensors, these results are ideal for the development of room temperature gas sensor [32].
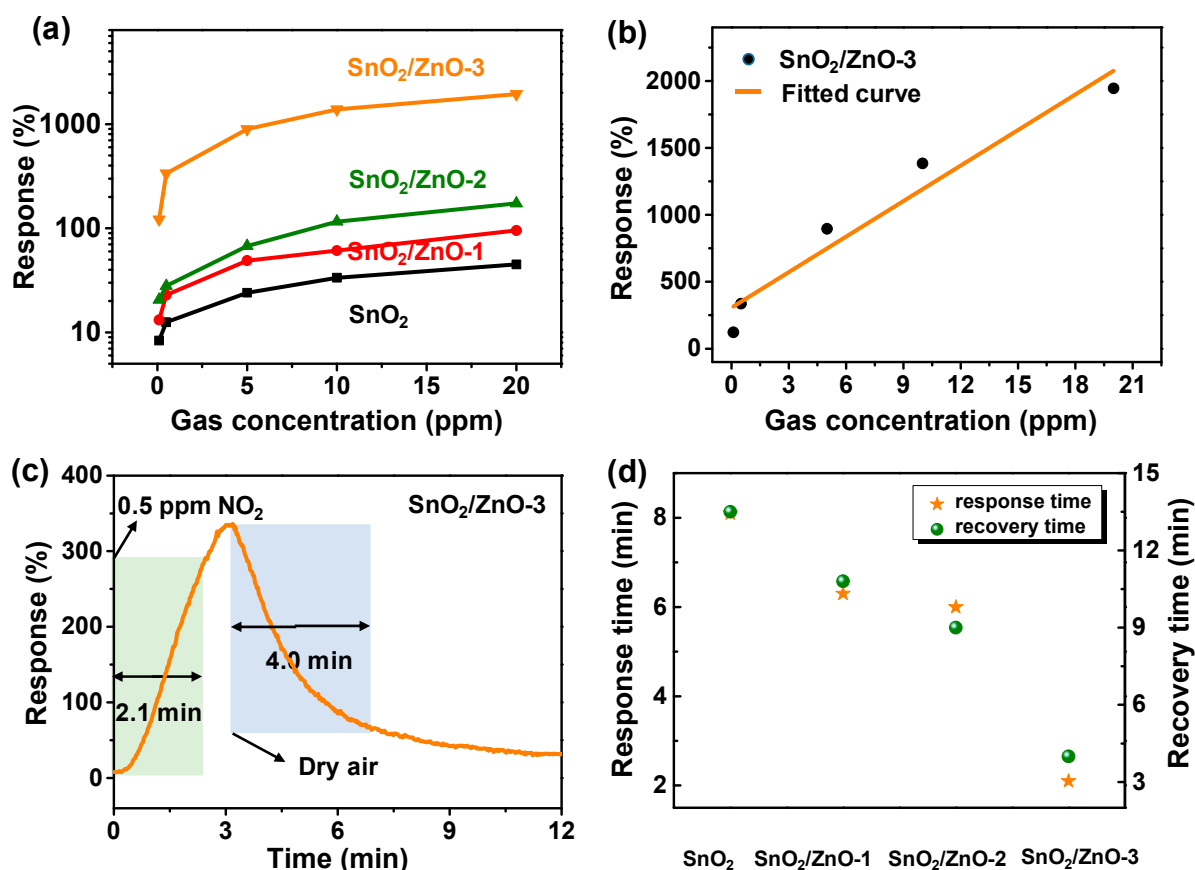
Figure 6. (**a**) Dynamic response curves to 0.1–20 ppm NO_2 gas at room temperature. (**b**) The linear range for NO_2 detection of SnO_2/ZnO-3 gas sensors. (**c**) Response and recovery time of SnO_2/ZnO-3 gas sensors to 0.5 ppm NO_2. (**d**) Response and recovery time of gas sensors based on as-prepared samples to 0.5 ppm NO_2.

Table 2. Comparison of the NO_2 sensing properties of different materials.

Materials	Method	°C	Response (%)	Concentration (ppm)	Response Time	Ref.
Au-WO$_3$	modified precipitation/ impregnation	250	836.6	5	64.2 s	[2]
Black Phosphorus	chemical exfoliation	RT	80	1	200 s	[33]
rGO-NiO	hydrothermal method	RT	100	15	300 s	[34]
MoS$_2$/Graphene	annealing process	100	12.5	0.5	10 min	[35]
rGO-ZnO	solution synthesis	RT	119	1	2.4 min	[36]
Sn-doped ZnO	successive ionic layer adsorption	150	10.5	1.5	20 min	[37]
SnO$_2$/ZnO	electrospin	RT	336.15	0.5	126 s	This work
SnO$_2$/ZnO	thermal evaporation	RT	239	1	-	[21]
SnO$_2$/ZnO	two–step hydrothermal	150	0.2	5 ppb	60 s	[30]
SnO$_2$/rGO	hydrothermal treatment	50	3.31	5	135 s	[6]
rGO-Cu$_2$O	nonclassic crystallization	RT	67.8	2	1000 s	[38]
rGO-Co$_3$O$_4$	hydrothermal method	RT	80	60	2 min	[39]

To investigate the repeatability of SnO_2/ZnO composites, the response performance of SnO_2/ZnO-3 sensor to 0.3 ppm of NO_2 was tested for four successive cycles at room temperature. As can be seen from Figure 7a, the baseline was fully capable of returning to its original position, and there was no significant difference in response values, an indication that SnO_2/ZnO-3 gas sensor had excellent repeatability. Figure 7b shows the enlargement of response and recovery time of SnO_2/ZnO-3 sensor to 0.3 ppm of NO_2. It was found that the response value was 135.7%, and the response/recovery times were 1.6

and 4.0 min, respectively. Selectivity is another fundamental characteristic of gas sensors. Figure 7c shows the selectivity of SnO_2/ZnO-3 gas sensor to 0.5 ppm of NO_2 and 150 ppm other gases under the same measurement conditions, including HCHO, CH_4, SO_2, C_8H_{10}, NH_3, and CO. The results indicate that the gas sensors based on SnO_2/ZnO-3 had low sensitivity (response value < 5) to other gases except when compared to the values obtained for NO_2.

When gas sensors are operated at room temperature, the effect of relative humidity on sensing properties should also be studied. To investigate the effect of humidity on both SnO_2 sensors and SnO_2/ZnO sensors, SnO_2 and SnO_2/ZnO-1 were tested in 5 ppm of NO_2 gas under 25–96% RH at room temperature (shown in Figure 7d). Both SnO_2 and SnO_2/ZnO sensors worked well and had a relatively stable sensing ability, demonstrating the good humidity resistance of sensors semiconductors. Moreover, the sensing measurements were repeated every few days at room temperature to investigate the stability of SnO_2/ZnO sensors. The results are shown in Figure 8, where the electrical signals of SnO_2/ZnO-3 sensors did not change dramatically after 18 days when detecting NO_2 gas. As can be seen in Figure 8d, after about ten days, the response value rose from about 250% at the beginning to about 300%, then gradually recovered and stabilized at about 250% with increasing number of days, an indication of the relatively good stability of the sensors.
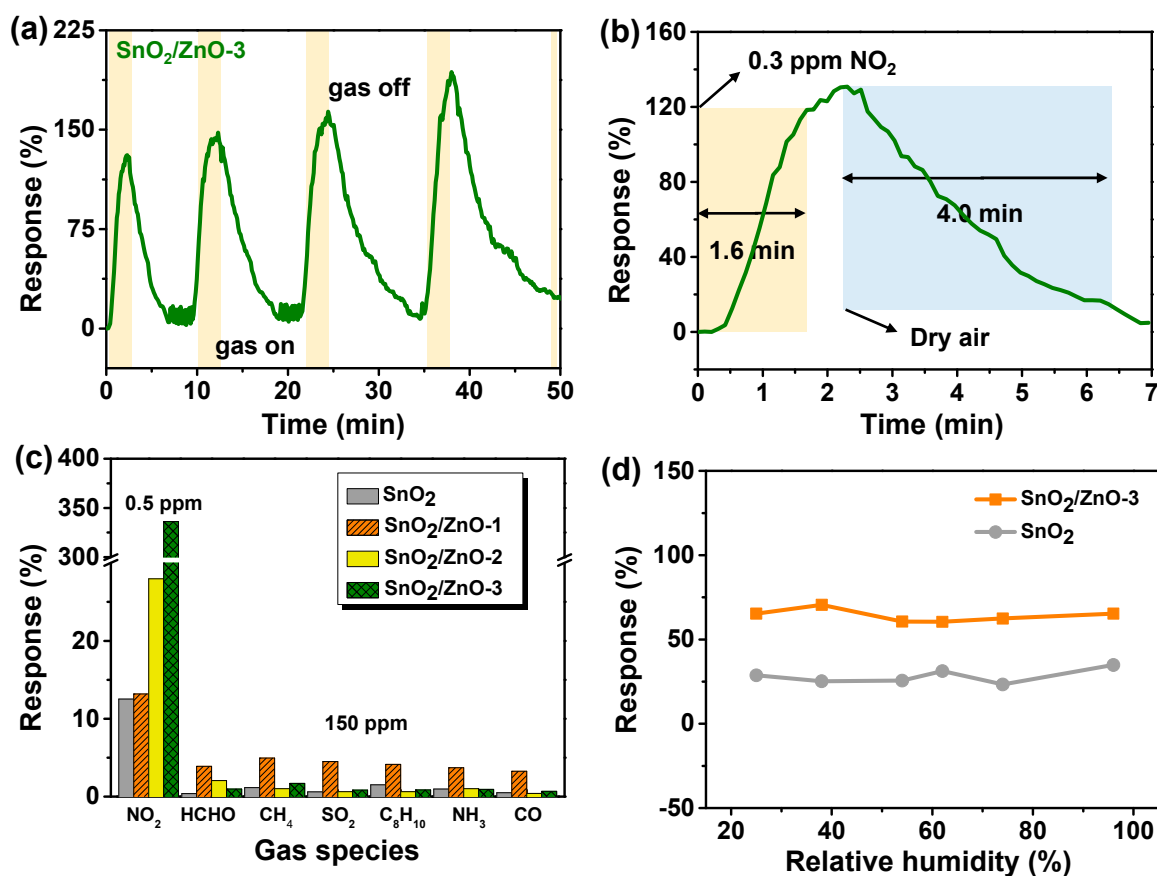

Figure 7. (**a**) Dynamic response of SnO_2/ZnO-3 gas sensors to 0.3 ppm NO_2 for four successive cycles. (**b**) Response and recovery time of SnO_2/ZnO-3 gas sensors to 0.3 ppm NO_2. (**c**) Selectivity of as-prepared samples sensors to 0.5 ppm NO_2 and 150 ppm other gases (HCHO, CH_4, SO_2, C_8H_{10}, NH_3, CO) under the same measurement condition. (**d**) Response vs. relative humidity of SnO_2, SnO_2/ZnO-3 sensors in 0.3 ppm NO_2.
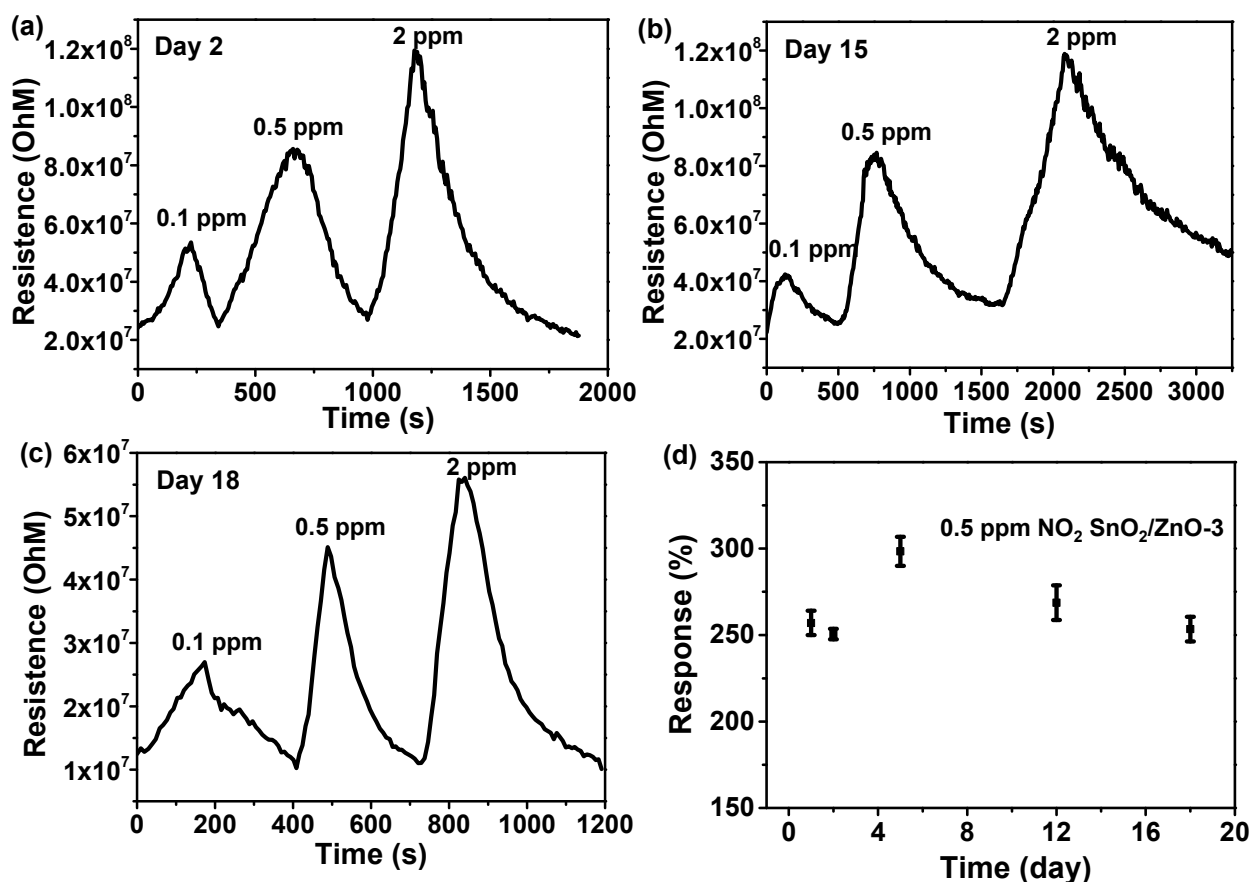
Figure 8. Resistance value of SnO_2/ZnO-3 sensors to 0.1, 0.5, 2 ppm NO_2 gas on the (**a**) second day, (**b**) 15th day, (**c**) 18th day. (**d**) The stability of SnO_2/ZnO-3 sensors to 0.1, 0.5, 2 ppm NO_2 gas within about 18 day.

3.3. Sensing Mechanism

During the process of NO_2 molecule adsorption, charge transfer can occur depending on the relative band positions of SnO_2/ZnO and NO_2, which can cause hybridization of NO_2 gas molecules state with SnO_2/ZnO nanocomposite orbitals. Such a charge transfer affects the resistance of SnO_2/ZnO, which can be facilely measured using a low-cost resistive transducing device. More importantly, physisorption of NO_2 molecules can occur at room temperature. When compared to pure SnO_2, SnO_2/ZnO has a larger electronegativity that could potentially enhance its gas adsorption sites [40,41]. On the other hand, the process of chemisorption can also modulate the resistance of sensing materials. A schematic diagram of the sensing mechanism of SnO_2/ZnO composite nanofibers to NO_2 gas is given in Figure 9. The significant improvement in sensing properties of SnO_2/ZnO composite nanofibers can be attributed to two factors. Firstly, the surface morphology, which is a parameter in sensing. The SnO_2/ZnO composite nanofibers contain more SnO_2 and ZnO nanoparticles than that of pure SnO_2 nanofibers. This led to larger surface area (38.7 m^2/g) in SnO_2/ZnO composite nanofibers, providing more adsorption sites for gas molecules. Secondly, the n-n heterojunction formed at the interface of SnO_2/ZnO composite nanofibers was also a reason for the enhanced gas sensing performance [42–45]. This phenomenon is illustrated in Figure 9a,b.

As shown in Figure 9a, the SnO_2/ZnO composite nanofibers were composed of SnO_2 and ZnO nanoparticles with different grain sizes. There was an energy barrier at the n–n heterojunction, which modulated the transport of electrons because of electron trapping. Figure 9b illustrates the energy band structure of SnO_2 and ZnO, in which E_f represents the Fermi level, E_g represents the energy band gap, and Φ, χ are working function and affinity, respectively. The resistance of SnO_2/ZnO gas sensor can be described using Equation (2):

$$R = R_0 exp\left(\frac{\Delta\Phi}{k_b T}\right) \tag{2}$$

where R_0 is a constant, k_b is the Boltzmann's constant, T is the absolute temperature, and $\Delta\Phi$ is the effective potential barrier, including heterojunction and homojunction barrier [30].
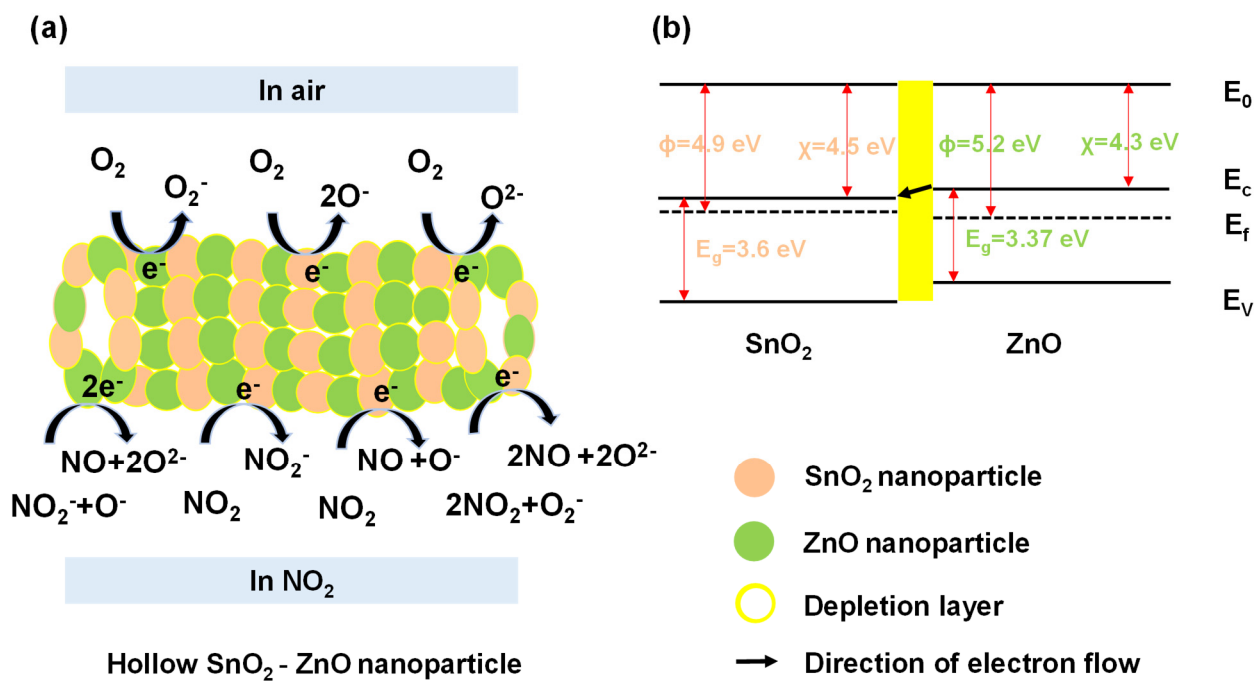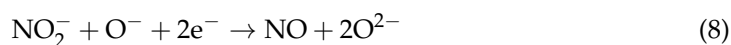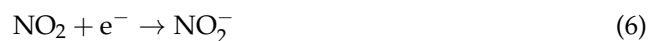

Figure 9. (**a**) Surface topography model of SnO_2/ZnO composite nanofibers. (**b**) Energy band structure of SnO_2/ZnO composite nanofibers.

In this context, oxygen molecules extracted electrons from the surface of SnO_2/ZnO nanofibers and formed oxygen ions (like O^-, O^-_2, O^{2-}) in the air, thereby leading to the formation of an electron depletion layer on SnO_2 and ZnO nanoparticles. The exact equations can be described using Equations (3)–(5):

$$O_2 + e^- \rightarrow O_2^- \tag{3}$$

$$O_2^- + e^- \rightarrow 2O^- \tag{4}$$

$$O^- + e^- \rightarrow O^{2-} \tag{5}$$
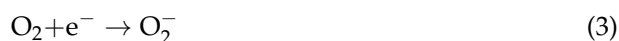
When NO_2 gas molecules were present, they extracted electrons from SnO_2, ZnO nanoparticles and oxygen ions because of stronger affinity to SnO_2/ZnO. This process widened the depletion layer and increased the resistance of the gas sensor. The surface electrochemical reaction was described using Equations (6)–(9):

$$NO_2 + e^- \rightarrow NO_2^- \tag{6}$$

$$NO_2 + e^- \rightarrow NO + O^- \tag{7}$$

$$NO_2^- + O^- + 2e^- \rightarrow NO + 2O^{2-} \tag{8}$$

$$2NO_2 + O_2^- + e^- \rightarrow 2NO + 2O_2^- \tag{9}$$

Therefore, it can be concluded that physisorption and chemisorption play an important role in controlling the gas-sensing performance of SnO_2/ZnO.

3.4. Integration and Gas Sensing Properties of Flexible Gas Sensors

The flexible electrodes were fabricated onto different flexible substrates integrated with SnO_2/ZnO composite nanofibers to form flexible wearable gas sensors. Figure 10a shows the shapes of the electrodes prepared by screen printing with silver paste on paper. The linear silver electrodes were bent to angles of 45°, 90° and 180° and then recovered (Figure 10b) during testing for adhesion between the silver lines and paper. The results obtained showed that the adhesion was strong enough to sustain bending at any angle. Furthermore, as seen in Figure 10c, the resistance of linear screen-printed electrodes only changed from 2.0 to 2.8 Ω after bending 10,000 times to an angle of 45°. Figure 11a–c show the photographs of flexible silver electrodes for gas sensor prepared by screen printing on PDMS, paper, and PET. The silver electrode was found to have closely bonded to the substrate. The edge of the line was also clear, proving that this study had successfully prepared flexible sensors.
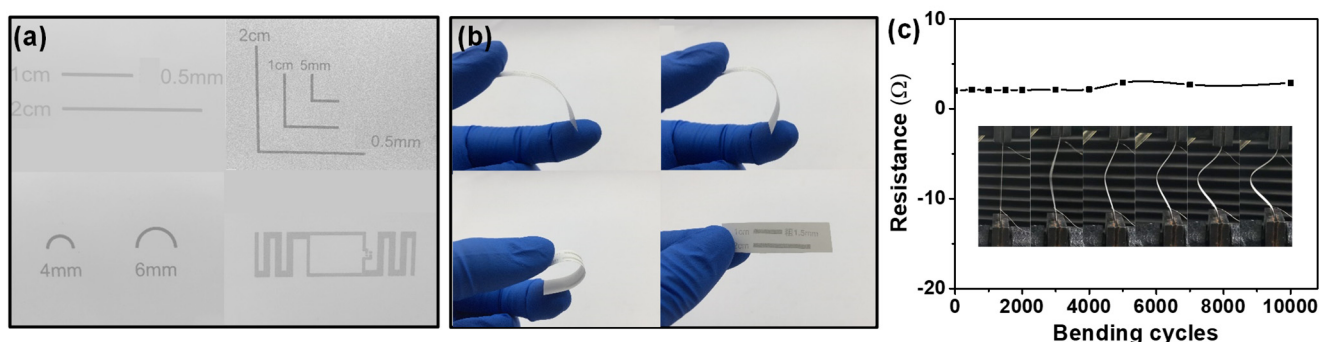

Figure 10. (**a**) Different shapes of electrodes prepared by screen printing with silver paste on paper. (**b**) Photographs of linear screen-printed silver electrodes bended at angles of 45°, 90°, 180° and recovered. (**c**) Resistance changes of linear screen-printed silver electrodes at angle of 45° bended for 10,000 times.
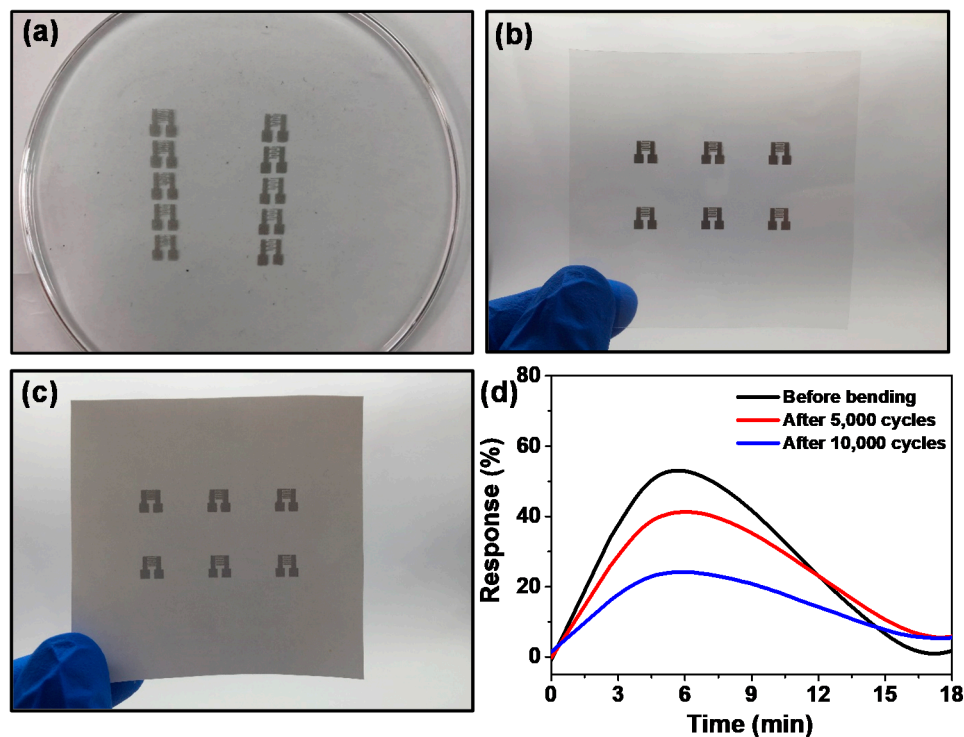

Figure 11. (**a**) Photograph of silver electrodes on PDMS. (**b**) Photograph of silver electrodes on paper. (**c**) Photograph of silver electrodes on PET. (**d**) Response and recovery curves of SnO_2/ZnO-3 gas sensors on flexible silver electrodes before and after 5000, 10,000 bending cycles in 0.1 ppm NO_2.

Figure 11d depicts the response and recovery curves of SnO_2/ZnO-3 gas sensors with flexible silver electrodes to 0.1 ppm of NO_2 before and after bending for 5000 and 10,000 cycles. The response values were 56%, 43% and 26%, respectively. Since the precision of screen printing is lower than that of the lithographic technique, the spacing of the interfingered electrodes was slightly larger, thereby increasing the difficulty of drop coating process. However, the idea of preparing flexible electrodes using screen printing could be extended to many other fields, such as EMI shielding [46], solar cells [47], and permanent memory devices [48]. The precision problems of screen printing can be improved through various methods such as filtration-assisted deposition [49].

4. Conclusions

Hollow SnO_2 nanofibers and SnO_2/ZnO composite nanofibers were successfully prepared through electrospinning and calcination in this work. When compared to pure SnO_2, gas sensors based on SnO_2/ZnO have higher sensitivity and selectivity to 0.5 ppm of NO_2 at room temperature, with a response value of 336%. This can be attributed to the heterojunction effect and the selective NO_2 physisorption sensing mechanism of SnO_2/ZnO nanocomposites. In addition, the increase of the specific surface area of SnO_2/ZnO-3 compared with pure SnO_2 also had a positive impact on the detection sensitivity. The response and recovery time of the SnO_2/ZnO sensors were two times shorter than those of pristine SnO_2 sensors. In addition, flexible electrodes were fabricated using screen printing and integrated with SnO_2/ZnO into a flexible gas sensor, then tested after 10,000 bending cycles. The flexible SnO_2/ZnO gas sensor was able to detect 0.1 ppm of NO_2 with a high response value of 56% at room temperature. This therefore shows that the fabrication strategy employed in this study is suitable for the development of flexible wearable sensing devices.

Author Contributions: Data curation, J.G. and Y.L.; Formal analysis, J.G. and H.H.; Methodology, J.G., W.L. and M.W.; Software, J.G. and X.Z.; Supervision, D.X., Y.Z. and H.Z.; Writing—original draft, J.G.; Writing—review & editing, J.G. All authors have read and agreed to the published version of the manuscript.

Conflicts of Interest: The authors declare no conflict of interest.

Sample Availability: Samples of the compounds are not available from the authors.

References

1. Xiao, B.; Song, S.; Wang, P.; Zhao, Q.; Chuai, M.; Zhang, M. Promoting effects of Ag on In_2O_3 nanospheres of sub-ppb NO_2 detection. *Sens. Actuators B Chem.* **2017**, *241*, 489–497. [CrossRef]
2. Kabcum, S.; Kotchasak, N.; Channei, D.; Tuantranont, A.; Wisitsoraat, A.; Phanichphant, S.; Liewhiran, C. Highly sensitive and selective NO2 sensor based on Au-impregnated WO_3 nanorods. *Sens. Actuators B Chem.* **2017**, *252*, 523–536. [CrossRef]
3. Zhang, J.; Zeng, D.; Zhu, Q.; Wu, J.; Huang, Q.; Zhang, W.; Xie, C. Enhanced room temperature NO_2 response of NiO-SnO_2 nanocomposites induced by interface bonds at the p-n heterojunction. *Phys. Chem.* **2016**, *18*, 5386–5396. [CrossRef] [PubMed]
4. Wang, Y.; Liu, C.; Wang, Z.; Song, Z.; Zhou, X.; Han, N.; Chen, Y. Sputtered SnO_2: NiO thin films on self-assembled Au nano-particle arrays for MEMS compatible NO_2 gas sensors. *Sens. Actuators B Chem.* **2019**, *278*, 28–38. [CrossRef]
5. Yuan, L.; Hu, M.; Wei, Y.; Ma, W. Enhanced NO_2 sensing characteristics of Au modified porous silicon/thorn-sphere-like tung-sten oxide composites. *Appl. Surf. Sci.* **2016**, *389*, 824–834. [CrossRef]
6. Zhang, H.; Feng, J.; Fei, T.; Liu, S.; Zhang, T. SnO_2 nanoparticles-reduced graphene oxide nanocomposites for NO2 sensing at low operating temperature. *Sens. Actuators B Chem.* **2014**, *190*, 472–478. [CrossRef]
7. Kumar, R.; Al-Dossary, O.; Kumar, G.; Umar, A. Zinc oxide nanostructures for NO_2 gas–sensor applications: A review. *Nano-Micro Lett.* **2015**, *7*, 97–120. [CrossRef] [PubMed]
8. Zhang, D.; Liu, Z.; Li, C.; Tang, T.; Liu, X.; Han, S.; Lei, A.B.; Zhou, C. Detection of NO_2 down to ppb Levels Using Individual and Multiple In_2O_3 Nanowire Devices. *Nano Lett.* **2004**, *4*, 1919–1924. [CrossRef]

9. Ruiz, A.M.; Sakai, G.; Cornet, A.; Shimanoe, K.; Morante, J.R.; Yamazoe, N. Cr-doped TiO₂ gas sensor for exhaust NO₂ moni-toring. *Sens. Actuators B Chem.* **2003**, *93*, 509–518. [CrossRef]

10. Bao, M.; Chen, Y.; Li, F.; Ma, J.; Lv, T.; Tang, Y.; Chen, L.; Xu, Z.; Wang, T. Plate-like p–n heterogeneous NiO/WO₃ nanocomposites for high performance room temperature NO₂ sensors. *Nanoscale* **2014**, *6*, 4063–4066. [CrossRef] [PubMed]

11. Malik, R.; Tomer, V.K.; Mishra, Y.K.; Lin, L. Functional gas sensing nanomaterials: A panoramic view. *Appl. Phys. Rev.* **2020**, *7*, 021301. [CrossRef]

12. Zhang, Y.; Kolmakov, A.; Lilach, Y.; Moskovits, M. Electronic control of chemistry and catalysis at the surface of an individual tin oxide nanowire. *J. Phys. Chem. B* **2005**, *109*, 1923–1929. [CrossRef] [PubMed]

13. Choi, K.J.; Hwang, I.-S.; Park, J.-G.; Lee, J.-H. Novel fabrication of an SnO₂ nanowire gas sensor with high sensitivity. *Nanotechnology* **2008**, *19*, 095508. [CrossRef]

14. Comini, E.; Cristalli, A.; Faglia, G.; Sberveglieri, G. Light enhanced gas sensing properties of indium oxide and tin dioxide sensors. *Sens. Actuators B Chem.* **2000**, *65*, 260–263. [CrossRef]

15. Li, W.; Guo, J.; Cai, L.; Qi, W.; Sun, Y.; Xu, J.-L.; Sun, M.; Zhu, H.; Xiang, L.; Xie, D.; et al. UV light irradiation enhanced gas sensor selectivity of NO2 and SO2 using rGO functionalized with hollow SnO2 nanofibers. *Sens. Actuators B Chem.* **2019**, *290*, 443–452. [CrossRef]

16. Choi, K.I.; Hübner, M.; Haensch, A.; Kim, H.J.; Weimar, U.; Barsan, N.; Lee, J.H. Ambivalent effect of Ni loading on gas sensing per-formance in SnO₂ based gas sensor. *Sens. Actuators B Chem.* **2013**, *183*, 401–410. [CrossRef]

17. Wan, G.X.; Ma, S.Y.; Li, X.B.; Li, F.M.; Bian, H.Q.; Zhang, L.P.; Li, W.Q. Synthesis and acetone sensing properties of Ce-doped ZnO nano-fibers. *Mater. Lett.* **2014**, *114*, 103–106. [CrossRef]

18. Li, W.; Teng, C.; Sun, Y.; Cai, L.; Xu, J.L.; Sun, M.; Li, X.; Yang, X.; Xiang, L.; Xie, D.; et al. Sprayed, scalable, wearable, and portable NO₂ sensor array using fully flexible AgNPs-All-Carbon nanostructures. *ACS Appl. Mater. Inter.* **2018**, *10*, 34485–34493. [CrossRef]

19. Miao, Y.-E.; He, S.; Zhong, Y.; Yang, Z.; Tjiu, W.W.; Liu, T. A novel hydrogen peroxide sensor based on Ag/SnO₂ composite nanotubes by electrospinning. *Electrochimica Acta* **2013**, *99*, 117–123. [CrossRef]

20. Wang, K.; Zhao, T.; Lian, G.; Yu, Q.; Luan, C.; Wang, Q.; Cui, D. Room temperature CO sensor fabricated from Pt-loaded SnO₂ porous nanosolid. *Sensors Actuators B Chem.* **2013**, *184*, 33–39. [CrossRef]

21. Park, S.; An, S.; Mun, Y.; Lee, C. UV-enhanced NO₂ gas sensing properties of SnO₂-core/ZnO-shell nanowires at room temperature. *ACS Appl. Mater. Inter.* **2013**, *5*, 4285–4292. [CrossRef] [PubMed]

22. Yang, T.; Gu, K.; Zhu, M.; Lu, Q.; Zhai, C.; Zhao, Q.; Yang, X.; Zhang, M. ZnO-SnO₂ heterojunction nanobelts: Synthesis and ultraviolet light irradiation to improve the triethylamine sensing properties. *Sens. Actuators B Chem.* **2019**, *279*, 410–417. [CrossRef]

23. Song, J.; Son, D.; Kim, J.; Yoo, Y.J.; Lee, G.J.; Wang, L.; Choi, M.K.; Yang, J.; Lee, M.; Do, K.; et al. Wearable force touch sensor array using a flexible and transparent electrode. *Adv. Funct. Mater.* **2017**, *27*, 1–9. [CrossRef]

24. Uddin, A.I.; Yaqoob, U.; Phan, D.-T.; Chung, G.-S. A novel flexible acetylene gas sensor based on PI/PTFE-supported Ag-loaded vertical ZnO nanorods array. *Sens. Actuators B Chem.* **2016**, *222*, 536–543. [CrossRef]

25. Secor, E.B.; Lim, S.; Zhang, H.; Frisbie, C.D.; Francis, L.F.; Hersam, M.C. Gravure printing of graphene for large-area flexible electronics. *Adv. Mater.* **2014**, *26*, 4533–4538. [CrossRef]

26. Hyun, W.J.; Secor, E.B.; Rojas, G.A.; Hersam, M.C.; Francis, L.F.; Frisbie, C.D. All-printed, foldable organic thin-film transistors on glassine paper. *Adv. Mater.* **2015**, *27*, 7058–7064. [CrossRef]

27. Zhang, J.; Wang, S.; Wang, Y.; Wang, Y.; Zhu, B.; Xia, H.; Guo, X.; Zhang, S.; Huang, W.; Wu, S. NO₂ sensing performance of SnO₂ hol-low-sphere sensor. *Sens. Actuators B Chem.* **2009**, *135*, 610–617. [CrossRef]

28. Ju, D.-X.; Xu, H.-Y.; Qiu, Z.-W.; Zhang, Z.-C.; Xu, Q.; Zhang, J.; Wang, J.-Q.; Cao, B.-Q. Near room temperature, fast-response, and highly sensitive triethylamine sensor assembled with au-loaded ZnO/SnO2 core–shell nanorods on flat alumina substrates. *ACS Appl. Mater. Interfaces* **2015**, *7*, 19163–19171. [CrossRef]

29. Lu, Z.; Zhou, Q.; Wang, C.; Wei, Z.; Xu, L.; Gui, Y. Electrospun ZnO-SnO₂ composite nanofibers and enhanced sensing properties to SF6 decomposition byproduct H2S. *Front. Chem.* **2018**, *6*, 540. [CrossRef]

30. Zhang, Z.; Xu, M.; Liu, L.; Ruan, X.; Yan, J.; Zhao, W.; Yun, J.; Wang, Y.; Qin, S.; Zhang, T. Novel SnO2@ZnO hierarchical nanostructures for highly sensitive and selective NO2 gas sensing. *Sens. Actuators B Chem.* **2018**, *257*, 714–727. [CrossRef]

31. Fan, H.J.; Knez, M.; Scholz, R.; Hesse, D.; Nielsch, K.; Zacharias, M.; Gösele, U. Influence of surface diffusion on the formation of hollow nanostructures induced by the kirkendall effect: The basic concept. *Nano Lett.* **2007**, *7*, 993–997. [CrossRef]

32. Joshi, N.; Hayasaka, T.; Liu, Y.; Liu, H.; Oliveira, O.N.; Lin, L. A review on chemiresistive room temperature gas sensors based on metal oxide nanostructures, graphene and 2D transition metal dichalcogenides. *Microchim. Acta* **2018**, *185*, 213. [CrossRef]

33. Cho, S.Y.; Lee, Y.; Koh, H.J.; Jung, H.; Kim, J.S.; Yoo, H.W.; Kim, J.; Jung, H.T. Superior chemical sensing performance of black phosphorus: Comparison with MoS₂ and graphene. *Adv. Mater.* **2016**, *28*, 7020–7028. [CrossRef]

34. Zhang, J.; Zeng, D.; Zhao, S.; Wu, J.; Xu, K.; Zhu, Q.; Zhang, G.; Xie, C. Room temperature NO2 sensing: What advantage does the rGO–NiO nanocomposite have over pristine NiO? *Phys. Chem. Chem. Phys.* **2015**, *17*, 14903–14911. [CrossRef]

35. Long, H.; Harley-Trochimczyk, A.; Pham, T.; Tang, Z.; Shi, T.; Zettl, A.; Carraro, C.; Worsley, M.A.; Maboudian, R. High surface area MoS2/Graphene hybrid aerogel for ultrasensitive NO2Detection. *Adv. Funct. Mater.* **2016**, *26*, 5158–5165. [CrossRef]

36. Xia, Y.; Wang, J.; Xu, J.-L.; Li, X.; Xie, D.; Xiang, L.; Komarneni, S. Confined formation of ultrathin ZnO nanorods/reduced graphene oxide mesoporous nanocomposites for high-performance room-temperature NO_2 sensors. *ACS Appl. Mater. Interfaces* **2016**, *8*, 35454–35463. [CrossRef]

37. Shishiyanu, S.T.; Shishiyanu, T.S.; Lupan, O. Sensing characteristics of tin-doped ZnO thin films as NO_2 gas sensor. *Sens. Actuators B Chem.* **2005**, *107*, 379–386. [CrossRef]

38. Deng, S.; Tjoa, V.; Fan, H.M.; Tan, H.R.; Sayle, D.C.; Olivo, M.; Mhaisalkar, S.; Wei, J.; Sow, C.H. Reduced graphene oxide con-jugated Cu_2O nanowire mesocrystals for high-performance NO_2 gas sensor. *J. Am. Chem. Soc.* **2012**, *134*, 4905–4917. [CrossRef]

39. Chen, N.; Li, X.; Wang, X.; Yu, J.; Wang, J.; Tang, Z.; Akbar, S. Enhanced room temperature sensing of Co_3O_4-intercalated reduced graphene oxide based gas sensors. *Sens. Actuators B Chem.* **2013**, *188*, 902–908. [CrossRef]

40. Ou, J.Z.; Ge, W.; Carey, B.; Daeneke, T.; Rotbart, A.; Shan, W.; Wang, Y.; Fu, Z.; Chrimes, A.F.; Wlodarski, W.; et al. Physisorption-based charge transfer in two-dimensional SnS_2 for selective and reversible NO_2 gas sensing. *ACS Nano.* **2015**, *9*, 10313–10323. [CrossRef]

41. Khan, H.; Zavabeti, A.; Wang, Y.; Harrison, C.J.; Carey, B.J.; Mohiuddin, M.; Chrimes, A.F.; De Castro, I.A.; Zhang, B.Y.; Sabri, Y.M.; et al. Quasi physisorptive two dimensional tungsten oxide nanosheets with ex-traordinary sensitivity and selectivity to NO_2. *Nanoscale* **2017**, *9*, 19162–19175. [CrossRef]

42. Li, W.; Ma, S.; Li, Y.; Yang, G.; Mao, Y.; Luo, J.; Gengzang, D.; Xu, X.; Yan, S. Enhanced ethanol sensing performance of hollow ZnO-SnO_2 core–shell nanofibers. *Sens. Actuators B Chem.* **2015**, *211*, 392–402. [CrossRef]

43. Huang, H.; Gong, H.; Chow, C.L.; Guo, J.; White, T.; Tse, M.S.; Tan, O.K. Low-temperature growth of SnO_2 Nanorod arrays and tunable n-p-n sensing response of a ZnO/SnO_2 Heterojunction for exclusive hydrogen sensors. *Adv. Funct. Mater.* **2011**, *21*, 2680–2686. [CrossRef]

44. Rakshit, T.; Santra, S.; Manna, I.; Ray, S.K. Enhanced sensitivity and selectivity of brush-like SnO_2 nanowire/ZnO nanorod heterostructure based sensors for volatile organic compounds. *RSC Adv.* **2014**, *4*, 36749–36756. [CrossRef]

45. Luo, Y.; Dong, Z.; Chen, Y.; Zhang, Y.; Lu, Y.; Xia, T.; Wang, L.; Li, S.; Zhang, W.; Xiang, W.; et al. Self-powered NiO@ZnO-nanowire-heterojunction ultraviolet micro-photodetectors. *Opt. Mater. Express* **2019**, *9*, 2775–2784. [CrossRef]

46. Dijith, K.S.; Pillai, S.; Surendran, K.P. Screen printed silver patterns on $La_{0.5}Sr_{0.5}CoO_{3-\delta}$—Epoxy composite as a strategy for many-fold increase in EMI shielding. *Surf. Coat. Technol.* **2017**, *330*, 34–41. [CrossRef]

47. Hösel, M.; Søndergaard, R.R.; Angmo, D.; Krebs, F.C. Comparison of fast roll-to-roll flexographic, inkjet, flatbed, and rotary screen printing of metal back electrodes for polymer solar cells. *Adv. Eng. Mater.* **2013**, *15*, 995–1001. [CrossRef]

48. Park, J.-H.; Park, M.-J.; Lee, J.-S. Dry writing of highly conductive electrodes on papers by using silver nanoparticle–graphene hybrid pencils. *Nanoscale* **2017**, *9*, 555–561. [CrossRef]

49. Juang, Y.-J.; Li, W.-S.; Chen, P.-S. Fabrication of microfluidic paper-based analytical devices by filtration-assisted screen printing. *J. Taiwan Inst. Chem. Eng.* **2017**, *80*, 71–75. [CrossRef]